Ga co-doping in Cz-grown silicon ingots to overcome limitations of B and P compensated silicon feedstock for PV applications

Maxime Forster, Erwann Fourmond, Roland Einhaus, Hubert Lauvray, Jed Kraiem, Mustapha Lemiti

Ga co-doping in Cz-grown silicon ingots to overcome limitations of B and P compensated silicon feedstock for PV applications.

Maxime Forster [*1,2], Erwann Fourmond[2], Roland Einhaus[1], Hubert Lauvray[1], Jed Kraiem[1] and Mustapha Lemiti[2]

[1] APOLLON SOLAR, 66 cours Charlemagne, 69002, Lyon, France
[2] INSA de LYON, INL, 7 av. J. Capelle, 69621 VILLEURBANNE CEDEX, France

Received ZZZ, revised ZZZ, accepted ZZZ
Published online ZZZ (Dates will be provided by the publisher.)

Keywords: Compensated silicon, Gallium co-doping

* Corresponding author: maxime.forster@insa-lyon.fr, Phone: +33(0)4 72 43 82 33, Fax: +33(0)4 72 43 85 31

In this paper, we investigate gallium co-doping during crystallisation of boron and phosphorus compensated Si. It is shown that the addition of gallium allows to obtain a fully p-type ingot with high resistivity despite high B and P contents in the silicon. Segregation of doping impurities is consistent with theory with a slight adjustment to take Ga evaporation into account. We have determined that 10 to 15% of P atoms are electrically inactive. Relatively high minority carrier lifetimes are measured in this material.

1 Introduction On the way to reduce the cost of solar energy, one promising path is the usage of low cost Si feedstock, or UMG-Si, obtained by simplified purification processes [1]. One drawback of UMG-Si is that it contains large amounts of both B and P, these impurities being the most difficult to remove through the metallurgical route. In such a compensated Si, electrical properties are differing from solely B-doped Si. Previous results [2] have shown the minority carrier lifetime to be higher and thus to give improved solar cell performances when the compensation level (C_l) was high i.e. for low net doping N_A-N_D (high resistivity). In addition, high C_l seems to have a positive effect on the so-called light-induced degradation observed in B-doped and oxygen contaminated Si [3,4]. However, because of the lower segregation coefficient of phosphorus (0.35) compared to that of boron (0.8), the net doping is not uniform along ingot height and an inversion of the Si polarity, from p- to n-type may occur during the crystallisation, reducing the material yield for industrial solar cell fabrication. Simulations [5] using the Scheil's law for the dopants distribution and simple models for the carrier mobility calculation show that a minimum resistivity of 0,5Ω.cm required for solar cell fabrication and an ingot yield of at least 90% implies the use of Si feedstock containing less than 0.45ppmw of B and 1.0ppmw of P. Gallium co-doping has recently been proposed [6-8] as a potential solution to control the C_l along the ingot height even when using Si containing large quantities of B and P. It relies on the low segregation coefficient of Ga which allows counterbalancing the increase of P concentration over that of B during crystal growth. This thus permits to obtain a low net doping and a p-type resistivity along the whole ingot height. This method has been experimentally validated [6] on a mc-Si ingot grown with Ga co-doped UMG-Si. A deeper understanding of the effect of the dopants distribution was however difficult to reach due to the presence of other impurities and crystal defects that are present in mc-Si. In this work, we explore the influence Ga co-doping on a Cz-Si crystal, grown with high purity solar grade Si to which was added known concentrations of B, P and Ga. The study focuses on the segregation effects during crystal growth and on the electrical properties dependence with the doping impurities concentrations, such as dopant activation and minority carrier lifetime.

2 Experimental details For this study, an <100> oriented Si ingot of about 160mm diameter was grown by the Cz method, using 15kg of Hemlock solar grade poly-Si free of doping impurities to which was added known concentrations of B, P and Ga (Table 1). The concentrations of

B and P correspond to a UMG-Si from which B has been efficiently removed by purification but which still contains relatively high amounts of P. The added Ga concentration is calculated using the Scheil equation in order to obtain a fully p-type ingot and a relatively high resistivity. B and P were introduced through highly doped Si wafers in which the doping impurity concentration was evaluated by means of 4-points probe resistivity measurements correlated to the Irvin curves. Ga was introduced in the form of high purity Ga particle grains. All the dopant sources were precisely weighed and put into the crucible together with the Si nuggets before fusion. The crystal was grown with an average pulling rate of v = 0.7 mm/min, a crystal rotation rate of $w_{cryst.}$ = 1.26 rad.s^{-1} and an inverse rotation of the crucible $w_{cruc.}$ = 0.84 rad.s^{-1} under an Ar pressure of 20 torr. The obtained ingot was then shaped into a 125x125 mm² pseudo-square brick and sliced into 240 µm thick wafers which were KOH etched to remove saw damages. SIMS analyses were carried out on wafers originating from different ingot heights in order to determine the doping impurities vertical distribution. 4-points probe resistivity and Hall effect measurements were performed to study the electrical activation of dopants. Minority carrier lifetimes were measured by QSSPC after chemical polishing and iodine ethanol passivation.

3 Results and discussion

3.1 Doping impurities distribution Figure 1 shows the evolution of resistivity, measured by 4-points probe, along the ingot height. The resistivity is plotted against the solidified fraction f_S until 0.85 since 15% of the initial Si melt mass remained in the crucible after crystallisation or was removed with the ingot tail. The measured resistivity is p-type along the whole ingot height and is comprised between 0,5 and 5,5 Ω.cm, this range being very well suited to the fabrication of good performance solar cells. SIMS analyses (Fig. 2) show that this p-type resistivity is to be attributed to the addition of Ga. Indeed, one can observe that P concentration is at each height over that of B, suggesting that without Ga co-doping, the ingot would be fully n-type.

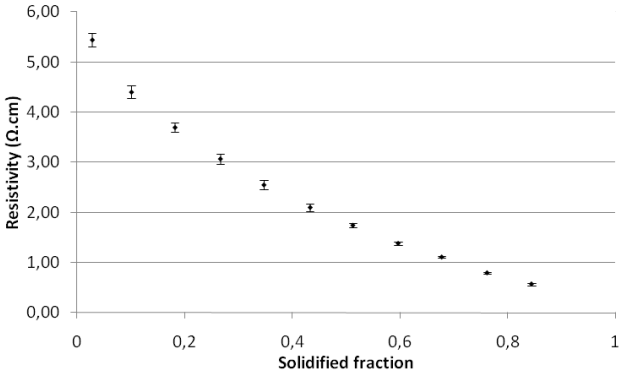

Figure 1 Resistivity averaged on 4-points probe measurements done at 5 different points of each wafers taken out from different ingot heights. Measured resistivity shows a good uniformity within the wafer's surface.

Table 1 Concentrations of B, P and Ga added to the Si melt before crystallisation.

Element	C_0 added to the melt (cm^{-3})	C_0 from Scheil (cm^{-3})	k_0	k_{eff} from Scheil	k_{eff} from BPS
Boron	2.67×10^{16}	1.99×10^{16}	0.80	0.771	0.818
Phosphorus	1.78×10^{17}	1.58×10^{17}	0.35	0.316	0.367
Gallium	5.79×10^{18}	3.54×10^{17}	0.008	0.105	0.0086

To study the axial distribution of doping impurities, the segregation coefficients k_{eff} of each impurity as well as their initial concentrations in the melt C_0 were extracted by fitting the Scheil's equation (1) to the experimental SIMS data,

$$C_S = k_{eff} \cdot C_0 \cdot (1 - f_S)^{k_{eff}-1} \quad (1)$$

where C_S is the concentration in the crystal at the solidified fraction f_S. In order to compare those results with theoretical values, B, P and Ga effective segregation coefficients were calculated for the growth conditions used in this work, with the equation (2) derived from the BPS theory [9],

$$k_{eff} = \frac{k_0}{k_0 + (1 - k_0) \cdot \exp(-\delta v / D)} \quad (2)$$

where k_0 is the equilibrium segregation coefficient, δ is the thickness of the diffusion layer in the Si melt near the solid to liquid interface and D is the diffusion coefficient of the impurity in the liquid phase. All the calculated k_{eff} and C_0 are reported in Table 1 together with the k_0 taken from [10].

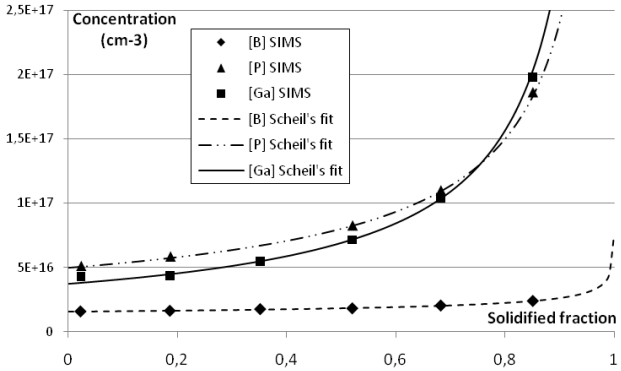

Figure 2 B, P and Ga distributions along the ingot height measured by SIMS. The continuous lines represent the fit to the Scheil's law.

The segregation coefficients of B and P extracted by fitting the Scheil's law are in good agreement with the BPS theory. However, the extracted initial concentrations in the

melt are slightly below the values expected from the doping sources that were introduced in the Si melt. The segregation coefficient of Ga derived from the fit to the Scheil's law is one order of magnitude higher than that calculated with the BPS theory. Such an increase of the effective segregation coefficient has already been observed in Ga-doped Si crystal co-doped with B [11]. This increase was explained, deriving the Thurmond and Struthers theory [12], by a potential Ga-B pair formation showing a better accommodation to the Si lattice and thus leading to an enhanced Ga incorporation during crystal growth. However, this interaction is unlikely to explain the increase of the Ga segregation coefficient observed here, since it is expected to occur at B concentrations higher than 1×10^{19} cm^{-3} and to reach a maximum k_{eff} of only 0.011 for very high B concentrations.

Another plausible explanation for the observed difference is the evaporation of Ga from the melt due to the low pressure conditions. Considering in such case that the quantity of evaporated Ga atoms per unit of time is given by (3), the Scheil's law has to be modified into the form (4),

$$\frac{dn_{Ga}}{dt} = E \cdot S_L \cdot C_L \tag{3}$$

$$C_S = k_{eff} \cdot C_0 \cdot (1 - f_S)^{k_{eff} + \frac{E \cdot S_L}{v \cdot S_C} - 1} \tag{4}$$

E being the evaporation rate, C_L the Ga concentration in the melt, S_L the free surface of the Si melt and S_C the surface of the crystal transversal section. The parameters obtained using this modified Scheil law (Fig.3) are shown in Table 2.

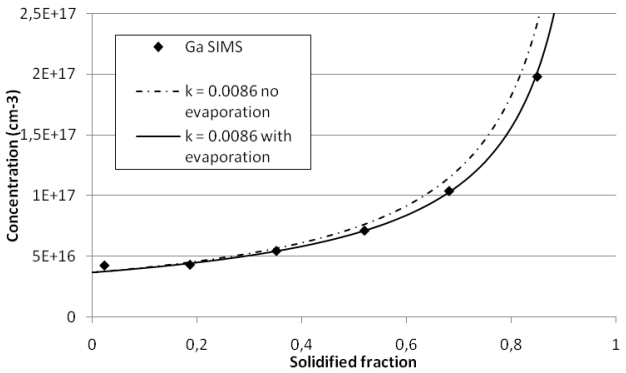

Figure 3 Axial distribution of Ga fitted with the Scheil's law taking into account evaporation from the melt. Dashed line displays the distribution of Ga expected from the Scheil's law without taking evaporation into account.

Table 2 k_{eff} and C_0 used for the fit of Ga distribution to the Scheil's law with and without taking evaporation into account.

	C_0 added (cm^{-3})	C_0 Scheil (cm^{-3})	k_{eff} BPS	k_{eff} Scheil	E (cm/s)
Fit without E	5.79×10^{18}	3.54×10^{17}	0.0086	0.105	0
Fit with E	5.79×10^{18}	4.63×10^{18}	0.0086	0.0086	2.7×10^{-5}

3.2 Doping impurities activation In order to evaluate the activation of dopants in this material, we executed Hall effect measurements on samples taken out from different ingot heights. The aim was to compare the majority carrier density to the net doping deduced from SIMS analyses. The difficulty to interpret Hall effect measurements arises from the fact that the measured Hall carrier density p_H differs from the true carrier density p by a factor close to unity (4), called the Hall factor r_H, which depends on the main scattering mechanism.

$$p = r_H \cdot p_H \tag{5}$$

r_H dependence with doping impurities concentration and temperature have already been studied for uncompensated p-type Si [13, 14]. Although no data was found in literature for r_H in highly compensated Si, recent results suggest that it is only weakly depending on the compensation level [15]. In this work, r_H will be assumed to be equal to 0.7 at ambient temperature for all the samples, as predicted for uncompensated p-type Si of similar doping impurities concentration. The validity of this assumption is discussed below.

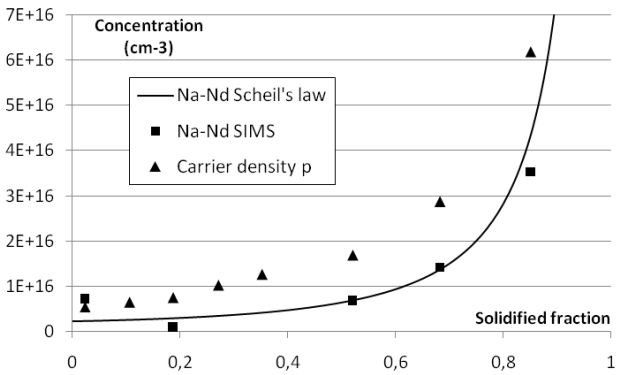

Figure 4 Evolution of the carrier density p measured by Hall effect and of the net doping N_A-N_D measured by SIMS with ingot height.

Fig.4 displays the evolution of the carrier density p together with the net doping N_A-N_D deduced from SIMS, both plotted against the solidified fraction. These results show that the measured carrier density p is systematically higher than the net doping N_A-N_D. One has to remember here that SIMS measurements provide the total dopant concentration, which can differ significantly from the activated dopant concentration located in substitutionnal position. Two hypothesis can explain the larger value of p compared to N_A-N_D: 1) the true Hall factor is smaller than that used to deduce p from p_H; 2) a certain quantity of P atoms are electrically inactive (interstitial position, precipitates or complexes formation).

The resistivity measurements (Fig.1) allow us to prefer the hypothesis 2). Indeed, assuming all dopants to be activated implies the carrier density to be inferior to N_A-N_D and thus the majority carrier mobility to be superior to a minimum μ_{min} calculated by (5):

$$\mu_{\min} = \frac{1}{(N_A - N_D) \cdot q \cdot \rho} \quad (6)$$

Such a calculation leads to some values for μ_{min} up to 690 cm²/V.s, values that are far over the theoretical limits predicted for uncompensated p-type Si of similar doping levels. It is thus very probable that the actual net doping, taking into account only the electronically activated dopants, is higher than that deduced from SIMS measurements, suggesting that 10 to 15% of the P atoms are inactive. As the P concentration in this material is significantly lower than the solubility limit, it can be inferred that the deactivation of P atoms is to be attributed to complexes or precipitates involving the contribution of other dopants or impurities.

3.3 Lifetime measurements QSSPC lifetime measurements were carried out to evaluate the impact of doping impurities on the electrical quality of Si. Results show that relatively high lifetimes are obtained in the top part of the ingot considering the quality of the Si feedstock. A continuous decrease of the minority carrier lifetime is observed with the increase of the solidified fraction (Fig. 5) which can be attributed, as proposed by Dubois et al. [2], to the increase of the majority carrier density and thus of the recombination strength of defects' energy states in the band gap of the Si. The very low carrier lifetimes measured in the bottom part of the ingot may also be attributed to the apparition of high densities of dislocations in this part of the ingot as was observed during crystal growth by the disappearance of the 4 facets on the edge of the ingot, representative of the dislocation-free <100> oriented mono-crystal.

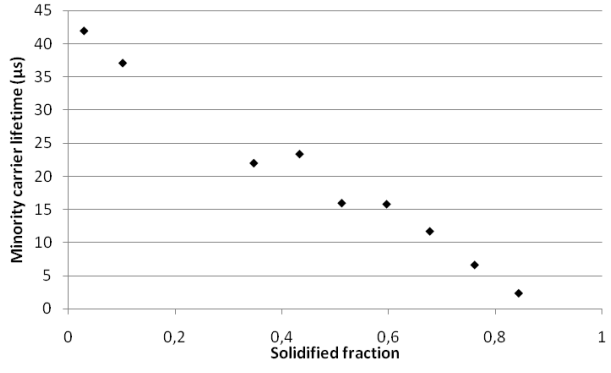

Figure 5 Evolution of the minority carrier lifetime measured for each sample at the injection level Δn = 0.1×p. The samples surfaces are passivated using an iodine ethanol solution.

3 Conclusion Gratefully to Ga co-doping we have managed to control the net doping along the ingot height during crystallisation of B and P compensated Si. This method may thus be used to increase the B and P concentration limits allowed in UMG-Si to produce high quality solar cells. The axial distribution of doping species was studied and showed a good agreement with theory. A slight adjustment of the Ga segregation profile can be attributed to an evaporation of Ga during crystal growth with a rate calculated to be equal to $E = 2.7\times10^{-5}$ cm/s. It was shown that 10 to 15% of the P atoms are electrically inactive. Solar cells are currently under processing in order to evaluate the photovoltaic potential of this material.

Acknowledgements The authors would like to thank SILTRONIX for the crystallisation of the Cz-Si ingot that was used in this work and Maxime Levaslot from IUT Lannion for the Hall effect measurements.

References

[1] R. Einhaus et al. PHOTOSIL Simplified production of solar silicon from metallurgical silicon in: Proceedings 21st PVSEC, Dresden, Germany, 2006.
[2] S. Dubois, N. Enjalbert, and J. P. Garandet, Appl. Phys. Lett. **93**, 032114 (2008).
[3] S. Dubois, N. Enjalbert, and J. P. Garandet, Appl. Phys. Lett. **93**, 103510 (2008).
[4] D. Macdonald, F. Rougieux, A. Cuevas, M. Di Sabatino and L. J. Geerligs, J. Appl. Phys. **105**, 093704 (2009).
[5] E. Enebakk, A. K. Søiland, J. T. Håkedal, R. Tronstad, in: 3rd Intenational Workshop on Crystalline Silicon Solar Cells, SINTEF/NTNU, Trondheim, Norway, 2009.
[6] J. Kraiem, R. Einhaus and H. Lauvray, in: Proceedings 34th IEEE Photovoltaic Specialists Conference, Philadelphia, USA, 2009.
[7] D. Macdonald and A. Cuevas in: 19th Workshop on Crystalline Silicon Solar Cells & Modules: Materials and Processes, NREL, Vail, Colorado, 2009.
[8] J. Kraiem, R. Einhaus and H. Lauvray, World patent WO/2009/130409
[9] J. A. Burton, R. C. Prim, W. P. Schlichter, J. Chem. Phys. **21**, 1987 (1953).
[10] F. A. Trumbore, Bell Syst. Tech. J. **39**, 205 (1960).
[11] X. Huang, M. Arivanandhan, R. Gotoh, T. Hoshikawa and S. Uda, J. Crystal Growth **310**, 3335 (2008).
[12] C. D. Thurmond and J. D. Struthers, J. Phys. Chem. **57**, 831 (1953).
[13] J. F. Lin, L. C. Linares and K. W. Teng, Solid-State Electron. **24**, 827 (1981).
[14] F. Szmulovicz, Phys. Rev. B. **34**, 4031 (1986).
[15] J. Veirman, S. Dubois, N. Enjalbert, J. P. Garandet, D. R. Heslinga and M. Lemiti, Solid-State Electron. **54**, 671 (2010).